Acta Oceanol. Sin., 2023, Vol. 42, No. 7, P. 64–78
https://doi.org/10.1007/s13131-023-2225-3
http://www.aosocean.com
E-mail: ocean2@hyxb.org.cn

Dynamic geomorphology and storm response characteristics of the promontory-straight beach—a case of Gulei Beach, Fujian

Chao Cao[1, 2, 3, 4], Zijian Mao[5], Feng Cai[1, 2, 3, 4], Hongshuai Qi[1, 2, 3, 4]*, Jianhui Liu[1, 2, 3], Gang Lei[1, 2, 3], Shaohua Zhao[1], Gen Liu[1]

[1] Third Institute of Oceanography, Ministry of Natural Resources, Xiamen 361005, China

[2] Key Laboratory of Marine Ecological Conservation and Restoration, Ministry of Natural Resources, Xiamen 361005, China

[3] Fujian Provincial Key Laboratory of Marine Ecological Conservation and Restoration, Xiamen 361005, China

[4] Fujian Provincial Station for Field Observation and Research of Island and Coastal Zone in Zhangzhou, Zhangzhou 363200, China

[5] School of Advanced Manufacturing, Fuzhou University, Jinjiang 362200, China

Received 17 October 2022; accepted 19 June 2023

© Chinese Society for Oceanography and Springer-Verlag GmbH Germany, part of Springer Nature 2023

Abstract

As one of the main areas of tropical storm action in the northwestern Pacific Ocean, South China experiences several typhoons each year, and coastal erosion is a problem, making the area a natural testing ground for studying the dynamic geomorphological processes and storm response of promontory-straight coasts. This study is based on three years of topographic data and remote sensing imagery of Gulei Beach and uses topographic profile morphology, single width erosion-accretion and mean change, combined with the Coastsat model to quantify the seasonal and interannual variability and storm response of the beach and to explain the evolution of shoreline change and beach dynamics geomorphology in the last decade. Gulei Beach has been in a state of overall erosion and local accretion for a long time, with relatively obvious cyclical changes; seasonal changes are also obvious, which are mainly characterized by summer accretion and winter erosion, with accretion at the top of the bay and accretion and erosion on the north and south sides of the bay corner, respectively; the seasonal erosion-accretion volume of the beach profile ranges from –80 m^3/m to 95.52 m^3/m, and the interannual erosion-accretion volume ranges from –69.09 m^3/m to 87.31 m^3/m. The response of beaches to typhoons with different paths varies greatly depending on the length, slope, orientation and scale of beach development. The large and gently developing Futou beach is less responsive to storms, while the less developed headlands in the southern Gulei Peninsula are more susceptible to disturbance by external factors and respond more strongly to typhoons. Storm distance is more influential than storm intensity. Under the influence of human activities, obvious erosion hotspots develop during normal weather, but storm processes produce redistribution of beach material patterns, and erosion hotspots disappear after storms. The results of this study enrich the theory of beach dynamics geomorphology and provide technical support for disaster prevention and mitigation, as well as ecological restoration of coastal zones.

Key words: promontory-straight beach, dynamic geomorphology, storm response, Gulei Peninsula

Citation: Cao Chao, Mao Zijian, Cai Feng, Qi Hongshuai, Liu Jianhui, Lei Gang, Zhao Shaohua, Liu Gen. 2023. Dynamic geomorphology and storm response characteristics of the promontory-straight beach—a case of Gulei Beach, Fujian. Acta Oceanologica Sinica, 42(7): 64–78, doi: 10.1007/s13131-023-2225-3

1 Introduction

Sandy beaches are an important part of the coastal zone and have become a gathering place for human recreation due to their rich sandy resources and scenic beauty. However, approximately 70% of sandy shorelines worldwide are in a state of erosion (Cai et al., 2009), with average erosion rates greater than 1 m/a, and in some areas, it is as high as 4–5 m/a (Komar, 1998; Xia et al., 1993); thus, the extent of erosion is still increasing. China has more than 18 000 km of continental shoreline from north to south (Cao et al., 2022a; Cai et al., 2022) and is among the countries with the most serious coastal erosion, with sandy shoreline erosion being the most serious (Luo et al., 2013), as approximately 50% of the sandy shoreline in China currently suffers from varying degrees of erosion (Tian et al., 2018; Yu and Chen, 2009; Li and Fu, 1992). Coastal erosion can have many negative impacts on coastal economic, social development and the marine ecological environment. Therefore, there is an urgent need to clarify the characteristics and evolutionary patterns of the dynamic geomorphic response of beaches to guide the prevention, mitigation, protection and restoration of coastal zones.

Coastal erosion has been studied since the beginning of the 20th century (Xia et al., 1993), and as research has progressed,

Foundation item: The National Natural Science Foundation of China under contract Nos 42076058 and 41930538; the National Key Research and Development Program of China under contract No. 2022YFC3106104; the Scientific Research Foundation of Third Institute of Oceanography, Ministry of Natural Resources under contract Nos 2023023 and 2019017.
*Corresponding author, E-mail: qihongshuai@tio.org.cn

many scholars gradually shifted from a static (Shepard and Inman, 1950; Davies, 1958) to a dynamic approach to coastal systems (Bagnold, 1940; Wright and Thom, 1977; Bascom, 1951), and over the past hundred years, a wealth of coastal erosion theories and protective measures have been developed (Young et al., 2009; Liu et al., 2016; Allen, 2000; Ravens et al., 2009; Mimura et al., 2010; Cai et al., 2009; Cao et al., 2022b). The sandy coast of China can be divided into promontory, straight and sand bar lagoon types. Straight beaches have a straight shoreline and a wide, gently sloping beach with a large length (Cai et al., 2005). Curved headland beaches, the main sandy coastal type, tend to be more stable than open beaches due to the sheltering effect of the headland (Wang, 2008). Although headland beaches are susceptible to erosion due to storm surge damage and human activities, it has been shown that the beach profile is in dynamic equilibrium due to the cyclic effects of storms and standing waves under the alternating effect of seasonal changes (Kuriyama and Yanagishima, 2016; Liu et al., 2022a). The specific manifestations of this process are closely related to the geographical location and morphology of headland bays (Medina et al., 1994; Diez et al., 2018). Studies on the headland beaches have focused on planform (McCormick, 1993; Hsu and Evans, 1989) and profile evolution, and have investigated the process of sandy coastal erosion and siltation through horizontal and vertical changes in sand transport, beach profile changes and shoreline morphology (Chen and Chen, 2002; Luo et al., 2000); the study of coastal systems has been extended from short-term extreme storm events (Cai et al., 2002, 2006; Qi et al., 2009; Guo et al., 2022) to long-period beach evolution patterns (Karunarathna et al., 2012; Shepard and Inman, 1950). For short-term extreme storm effects, the study was carried out on beaches with different orientations, different coastal types and different storms, revealing the differences in responses to storms and the causes of storms on beaches with different orientations (Cai et al., 2002) and on both sides of a tropical cyclone (Cai et al., 2004), as well as the response characteristics of different coastal landform types to typhoons (Cai et al., 2006; Guo et al., 2022). Long-term topographic and geomorphological monitoring was used to analyse the morphological evolution of the shoreline and trends in accretion in terms of profile, shoreline, grain size and in conjunction with the hydrodynamic environment (Tian et al., 2018; Miller and Dean, 2007a, b). The multidimensional monitoring of elements at different spatial and temporal scales, combined with the evaluation and prediction of various coastal evolution models, such as the Coastsat model, provides an innovative means to explore the migration and transformation patterns and evolution trends of headland bays and rapids under the combined influence of global climate change and human activities.

The Gulei Peninsula is bordered by the sea on three sides, with a large headland and several small headlands on the eastern and southern sides of the peninsula, respectively, and the different orientations of the headlands produce significant variability in weather conditions. However, there are few analyses of the dynamic geomorphological response of the Gulei Peninsula beaches in China, and some studies have explored the beach flushing and accretion changes through sediment grain size changes (Wang et al., 2011), concluding that the Gulei Peninsula Futou Bay beach is a transitional beach (Liu et al., 2014). Other scholars have also analysed the impact of Typhoon Aere's landfall on beach erosion in Futou Bay and concluded that there were differences in the responses of different areas of Futou Bay beaches to the storm (Cai et al., 2006; Li et al., 2007). Most of these studies have focused on the erosion characteristics of Futou Bay on the eastern side of the Gulei Peninsula and the beaches along the outer edge of the local villages on the Gulei Peninsula, but no studies have been conducted on the promontory-straight beaches in the main part of the Gulei Peninsula. Therefore, this paper analyses the dynamic geomorphological characteristics of the beaches on the eastern and southern sides of the Gulei Peninsula based on medium- and long-term observation cycles and explains the response mechanisms of the promontory-straight beaches to different weather processes and different typhoon landing paths, which enriches the dynamic geomorphological theory of the promontory-straight beaches and provides technical support for disaster prevention and mitigation, as well as ecological restoration of the coastal zone in the region.

2 Materials and methods

2.1 *Overview of the study area and typhoons*

2.1.1 *Overview of the study area*

The Gulei Peninsula is in Gulei Town, Zhangzhou City, Fujian Province (23°43′–23°58′N, 117°33′–117°44′E) (Fig. 1) and is the largest structured continuous island sand bar in the southeast coastal region of China. The Gulei Peninsula is surrounded by sea on three sides, with Futou Bay to the east, Dongshan Bay to the west, and the Taiwan Strait to the south. The peninsula is 17.3 km long from north to south and has a width of approximately 3–4 km from east to west, covering an area of 40 km^2 (Wang et al., 2011). The study area is located at Futou Bay beach and extends from Ao'tou Mountain to Xia'an Village beach on the Gulei Peninsula (Fig. 1c). There are typical differences in planform between Futou Bay and the smaller small headland beaches to the south. Futou Bay (W1) starts from the northern end of the peninsula and ends at Ao'tou Mountain in the south. The bay has a NE–SW curved shape and is open towards the ESE, which is a typical straight beach. The area between Ao'tou Mountain and Xia'an Village Beach is located at the end of the Gulei Peninsula and is divided into four small promontory beaches by several headlands, each within 0.8 km to 2 km in length. From north to south, these include Ao'tou Mountain to Nei'nanyu shore (W2), Nei'nanyu to Hu'weicun Village shore (W3), Gu'cheng Village shore (W4), and Xia'an Village shore (W5). Since the 1950s, the coast of the Gulei Peninsula has been damaged by both strong typhoons and human activities. According to previous studies and field visits, the central part of Futou Bay has been in a state of continuous accretion in recent decades, with the beach silting up to 10 m into the sea (Cai et al., 2006). The vegetation along the southern backwaters of Futou Bay has been severely damaged by artificial means, and the coastal dunes have been extensively modified, with the modification of a large flood drainage channel.

The study area has a subtropical maritime monsoon climate and is significantly influenced by monsoons, with significant seasonal changes in wind direction (Xia, 2015). In summer, the SW monsoon influences the formation of southerly waves (S, SE), while in winter, the NE monsoon influences the formation of easterly waves (E, NE). The study area is dominated by NE winds from September to May and by SW winds from June to August in summer, with the most NE winds (26% frequency) throughout the year (Xia, 2015), with mean wind speeds averaging approximately 7.1 m/s. The maximum wind speed occurs in winter, and the minimum wind speed occurs in summer. From 1990 to 2008, 43 typhoons landed or affected the study area, with an average of approximately 1.54 typhoons impacting the location each year.

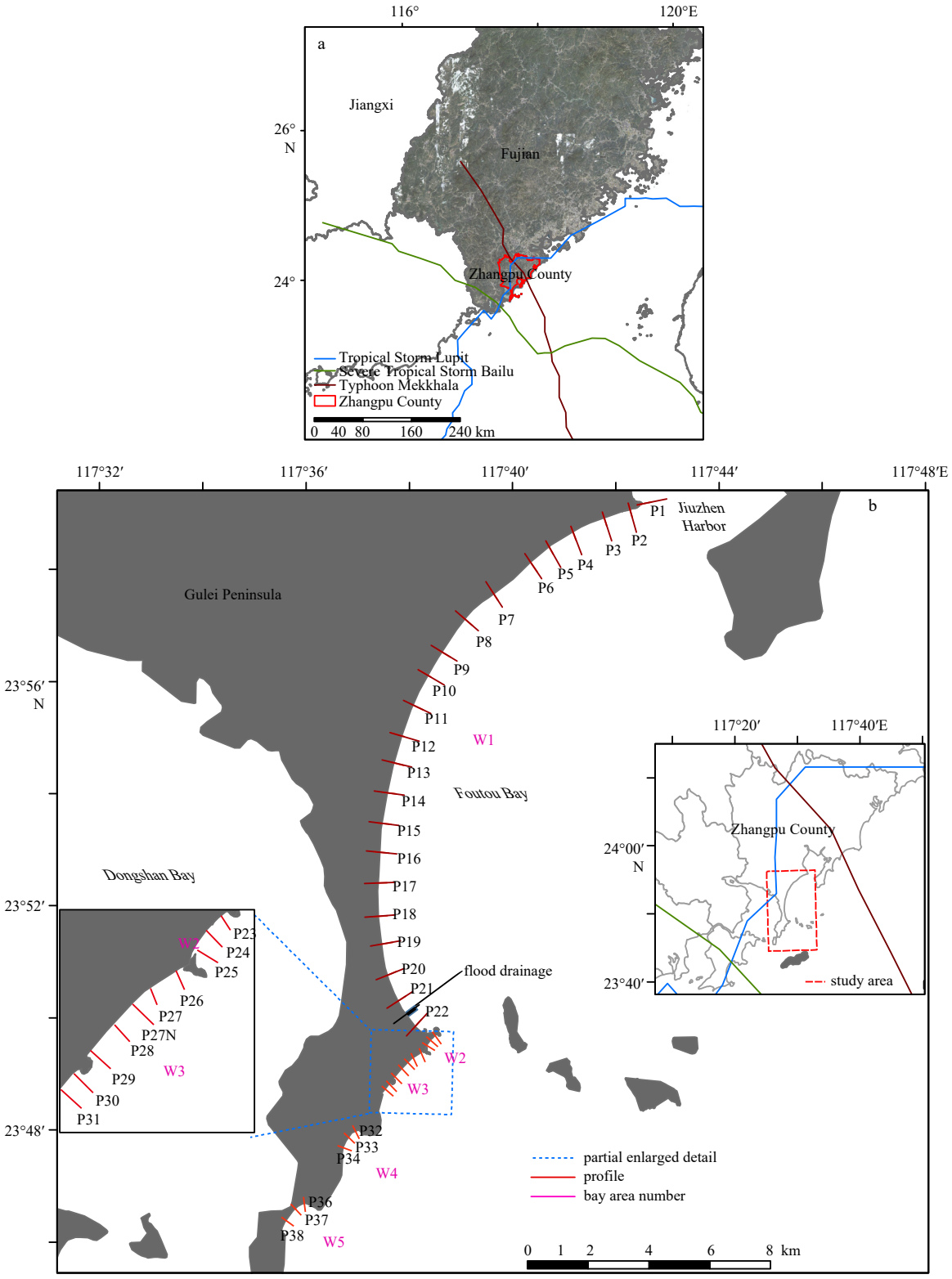

Fig. 1. Location of the study area, No. 11 Severe Tropical Storm Bailu Landing Path on August 25, 2019 (green color), and No. 6 Typhoon Mekkhala Landing Path on August 11, 2020 (brown color) and No. 9 Tropical Storm Lupit Landing Path on August 5, 2021 (blue color).

July to September is the season with the highest occurrence of typhoons (Xia et al., 2014). The average tidal difference in the study area is 2.4 m, which is a medium tidal area with a regular semidiurnal tide type. The beach sediments in the study area are dominated by medium-fine sands (Cai, 1989), with thin layers of coarse sands only in the surface layer of the seashore sandbank, and the median grain size mainly ranges from Φ = 0.32 to Φ = 2.07 based on field sampling and indoor particle size analysis.

2.1.2 *Typhoon overview*

During the monitoring period, the study area experienced three typhoons that made landfall from different paths. According to the wind field model (Young and Sobey, 1980), Severe Tropical Storm Bailu made landfall on the left side of the study area with a maximum wind force of 10 at landfall, and the wind direction in the study area changed from NNE to NEE during landfall, with a maximum instantaneous wind speed of 26.18 m/s near landfall. Typhoon Mekkhala made landfall on the right side of the study area, with maximum winds with a force of 12 at landfall. The wind direction in the study area shifted from NEE to N and finally to WNW, with a maximum instantaneous wind speed of 32.61 m/s at landfall. Tropical Storm Lupit made landfall from behind the study area, with maximum winds with a force of 8 at landfall. The wind direction in the study area changed from ESE to NW, with a maximum instantaneous wind speed of 20.96 m/s at landfall (Fig. 2).

2.2 *Field observations*

Seasonal, interannual and posttyphoon monitoring of the shoreline and 38 beach profiles (Fig. 1 and Table 1) in the study area was carried out from 2019–2021 using RTK-CORS measurements. Measurements were carried out at ±0.05 m in planimetric error and ±0.03 m in elevation error. Beach profiles were selected for measurement at low tide, starting at the boundary line of the protective forest and following the vertical coastline until near the low tide line, with points generally spaced at 0.5–1 m intervals and more points in areas with large topographic relief. The frequency of the measurements is 2–3 times per year, with a total of 8 monitoring periods (Table 1), where the two summer measurements represent the beach profile and shoreline changes before and after typhoons, respectively. The December and January measurements represent the winter coastal changes. During the three field surveys in December 2019, June 2020, and August, we also collected sediment samples from both the high-tide zone near the P14 profile in central Futou Bay and the low-tide zone, for a total of six samples.

2.3 *Data processing*

Using the beach profile comparison method, the topographic profile morphology of the same profile was plotted for multiple periods using CAD software to compare the topographic changes at the same location for different periods and calculate the single width erosion-accretion (UED) of the profile. Moreover, the definition of the mean change in beach profile (MPC) by Qi et al. (2010) was used to introduce the mean change in beach profile to characterize the seasonal shift and typhoon response intensity of the beach. Remote sensing images were used to extract the shoreline for the last 10 years, and after tidal correction, the Coastsat tool (Vos et al., 2019) was used to calculate the erosion-accretion variation in the shoreline in the study area for the last 10 years. Orangin software was used to create an erosion-accretion heatmap of the shoreline variation data for the last 10 years. The four types of data processing mentioned above were used to decipher the information on the change pattern of the shoreline and topographic profile, single-width erosion-accretion volume, and average change volume in the study area. The beach sediment samples were sieved according to the Taylor standard sieving system, the particle size parameters were calculated using the Folk-Ward (Folk and Ward, 1957) particle size parameter equation, the particle size standards were calculated using the Udden-Wentworth (Wentworth, 1922) isometric Φ-value particle size standard, and beach particle size accumulation maps were produced.

3 Results

3.1 *Sediment characteristics*

As seen from the beach grain size mapping, the sediments in the study area are dominated by fine sands, with median grain sizes mainly ranging from Φ = 0.89 to Φ = 2.07 (Fig. 3). In summer, the high tide area is dominated by fine sand with excellent sorting, and the grain size gradually increases seaward to the low tide area; in winter, with enhanced hydrodynamics, some of the coarse grains in the subtidal zone are transported to the supratidal zone, and there is coarsening of sediments in the high tide area, while the subtidal zone becomes relatively fine; in a stormy environment, the coarse grain sediment content in the high tide area is the highest, reaching 33%, and the sediments are obviously coarsened with poor sorting. The fine-grained sediments in the mid-tide supratidal zone are transported to the low-tide zone by the offshore currents, causing the sediment in the low-tide zone to become finer than in the high-tide zone.

3.2 *Characteristics of beach evolution at medium and long time scales*

The shoreline data of Futou Bay beach for the past 10 years were extracted from remote sensing images, and 240 transects were laid out along the shoreline (Fig. 4a) to calculate the shoreline variation trend and create a coastal erosion heatmap by Coastsat software. The erosion-accretion of the beach at Futou Bay showed high vertical variability and stable horizontal variab-

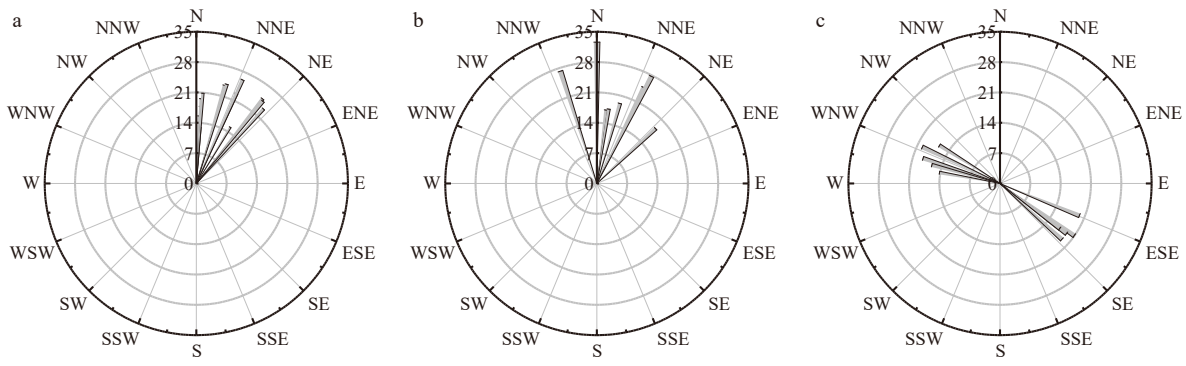

Fig. 2. Three typhoons' wind direction and maximum instantaneous wind speed (m/s), Severe Tropical Storm Bailu's wind direction and maximum instantaneous wind speed (a), Typhoon Mekkhala's wind direction and maximum instantaneous wind speed (b), Tropical Storm Lupit's wind direction and maximum instantaneous wind speed (c).

Table 1. Basic information of the beach profile

Profile name	Bar area number	Latitude and longitude of the stake point	Azimuth	Length/m	Measurement time
GL-P1	W1	23°57′06.38″N, 117°42′29.05″E	78°21′36.36″	150.18	2019–08–07 2019–08–26 2019–12–23 2020–06–15 2020–08–12 2021–01–27 2021–06–07 2021–08–07
GL-P2		23°57′02.50″N, 117°42′20.54″E	164°28′37.54″	63.56	
GL-P3		23°56′53.09″N, 117°41′50.67″E	162°17′59.84″	57.52	
GL-P4		23°56′37.13″N, 117°41′14.45″E	158°17′42.84″	29.28	
GL-P5		23°56′22.97″N, 117°40′45.87″E	150°15′55.85″	62.89	
GL-P6		23°56′07.17″N, 117°40′23.67″E	145°58′15.19″	213.26	
GL-P7		23°55′33.52″N, 117°39′40.66″E	147°52′30.01″	76.16	
GL-P8		23°55′05.89″N, 117°39′07.27″E	131°06′56.00″	119.34	
GL-P9		23°54′30.56″N, 117°38′40.01″E	121°29′41.15″	114.93	
GL-P10		23°54′04.92″N, 117°38′24.64″E	120°21′04.71″	118.50	
GL-P11		23°53′33.40″N, 117°38′07.10″E	115°21′45.80″	145.10	
GL-P12		23°53′00.79″N, 117°37′52.17″E	106°45′36.41″	150.57	
GL-P13		23°52′31.75″N, 117°37′43.80″E	103°30′14.58″	122.44	
GL-P14		23°51′59.78″N, 117°37′35.47″E	98°03′57.87″	103.27	
GL-P15		23°51′27.15″N, 117°37′28.98″E	96°42′02.30″	109.54	
GL-P16		23°50′56.02″N, 117°37′26.29″E	95°27′14.57″	98.02	
GL-P17		23°50′23.12″N, 117°37′24.81″E	88°08′32.02″	71.81	
GL-P18		23°49′47.41″N, 117°37′25.03″E	85°28′47.43″	79.67	
GL-P19		23°49′17.58″N, 117°37′29.70″E	79°37′17.19″	120.76	
GL-P20		23°48′44.23″N, 117°37′35.58″E	68°01′55.01″	111.35	
GL-P21		23°48′16.04″N, 117°37′46.92″E	57°04′02.82″	111.08	
GL-P22		23°47′48.09″N, 117°38′06.69″E	41°56′07.28″	129.43	
GL-P23	W2	23°47′39.72″N, 117°38′31.01″E	144°49′21.89″	101.36	
GL-P24		23°47′34.72″N, 117°38′25.39″E	130°35′57.87″	79.05	
GL-P25		23°47′29.19″N, 117°38′21.09″E	122°02′33.06″	75.73	
GL-P26	W3	23°47′21.33″N, 117°38′14.82″E	157°31′11.68″	86.46	
GL-P27		23°47′16.53″N, 117°38′05.02″E	154°46′43.47″	98.00	
GL-P27N		23°47′10.71″N, 117°37′59.39″E	136°28′57.29″	71.14	
GL-P28		23°47′04.29″N, 117°37′52.17″E	136°28′43.38″	72.26	
GL-P29		23°46′55.80″N, 117°37′44.05″E	135°38′30.34″	78.47	
GL-P30		23°46′48.10″N, 117°37′37.64″E	135°43′02.66″	102.84	
GL-P31		23°46′42.78″N, 117°37′32.65″E	131°42′13.80″	109.45	
GL-P32	W4	23°45′57.48″N, 117°36′57.93″E	153°07′32.19″	30.81	
GL-P33		23°45′51.31″N, 117°36′49.86″E	134°15′07.23″	44.69	
GL-P34		23°45′40.09″N, 117°36′43.54″E	110°18′02.60″	60.72	
GL-P36	W5	23°44′42.26″N, 117°35′57.79″E	173°29′29.27″	89.79	
GL-P37		23°44′35.99″N, 117°35′46.40″E	137°14′59.00″	86.97	
GL-P38		23°44′23.20″N, 117°35′35.72″E	126°06′42.76″	98.55	

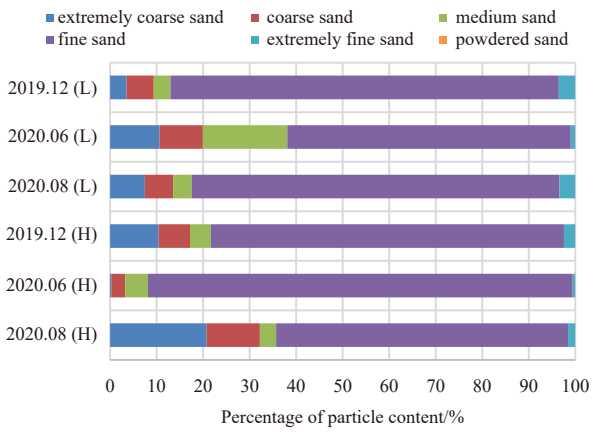

Fig. 3. Cumulative mass map of beach particle size. "L" represents samples taken from low tide areas, "H" represents samples taken from high tide areas.

ility with high local variability (Fig. 4b). Longitudinally, the northern and central parts of Futou Bay beach show significant accretion, while in the south, more pronounced erosion occurs, with the top of the bend gradually becoming less silty and showing erosion towards the sides. Horizontally, the change in erosion-accretion at Futou Bay beach shows a clear cyclical pattern but with different distribution trends. Locally, erosion hotspots appear in approximately 2013 and 2015 for the P15–P16 and P18–P20 shores, respectively, before disappearing and returning to equilibrium. More pronounced erosion occurred in association with the extension of the flood channel in this section in 2019.

3.3 *Characteristics of interannual variability in beaches*

The interannual variation in beaches in the study area shows significant differences in Futou Bay as well as the southern headland bay. In Bay W1, the average interannual beach profile variation in summer ranges from 0.12 m to 0.53 m, most of the variation is less than 0.2 m, and the beach surface variation is relatively small. Erosion is greater along the foreshore and hindshore,

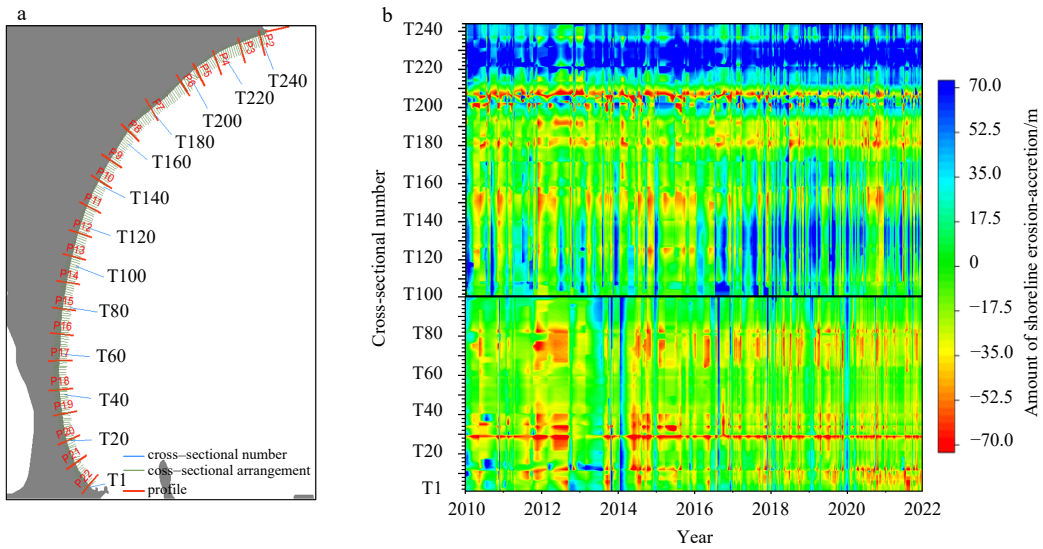

Fig. 4. Futou bay cross-section layout and shoreline evolution since 2010, the cross-section in Futou Bay are spaced at 100 m intervals and a total of 244 cross-section are laid out, with progressively smaller section numbers from north to south, with T240 located near Profile P2 and T1 in the southernmost part of Futou Bay (a), red in the figure represents receding shoreline erosion and blue represents advancing shoreline accretion (b).

with a maximum downwards erosion of nearly 2 m and a maximum erosion retreat of nearly 10 m; the subtidal zone is more stable, with significant development of submerged sand dams (P1 in Fig. 5); accretion occurs in central W1, with more significant accretion in 2020–2021 than in 2019–2020; the two interannual variations differ significantly around the P21 profile. The beach profiles in the four southern bays are more variable, with an average variation of 0.24–0.72 m and double beach shoulders forming in some profiles (P26 in Fig. 5). The amount of siltation gradually increases from north to south in each bay, with the largest change in beach shoulders in Profile P29, extending nearly 20 m seaward (P29 in Fig. 5), and the interannual variation trends are consistent between the two summers.

The interannual variation in single-width erosion and siltation is calculated as shown in Fig. 6, and the interannual variation in beaches in the study area mainly shows accretion. The difference between summer erosion-accretion in 2019–2020 and 2020–2021 is large. The summer of 2019–2020 shows slight erosion, with larger erosion in profiles P21, P32 and P34, with single-width erosion of 66.24 m^3/m, 69.09 m^3/m, and 55.84 m^3/m, respectively, with an average single-width erosion of 1.59 m^3/m across the shoreline. The summer of 2020–2021 shows greater accretion, with an average single-width accretion of 6.89 m^3/m.

The winter interannual variation in the beaches in the study area is relatively similar to the summer and long cycle variation (Fig. 6d), with a cumulative single width erosion-accretion of 134.65 m^3/m, generally showing accretion, with W1 being more stable than the southern bays. Within Bay W1, the Pl profile is highly eroded with a single width erosion of 60 m^3/m, with overall subtidal erosion and nearly 10 m of beach shoulder recession. The central part shows accretion, with overall accretion of the beach surface or subtidal accretion, with the subtidal slope becoming larger and the subtidal zone becoming slower. The Profiles P21 and P22 show very different interannual variability from the summer of 2019–2020. In the four southern bays, the interannual variation in winter is similar to that in summer, with more dramatic shoreline changes, showing a shift from erosion to siltation and a gradual increase in accretion.

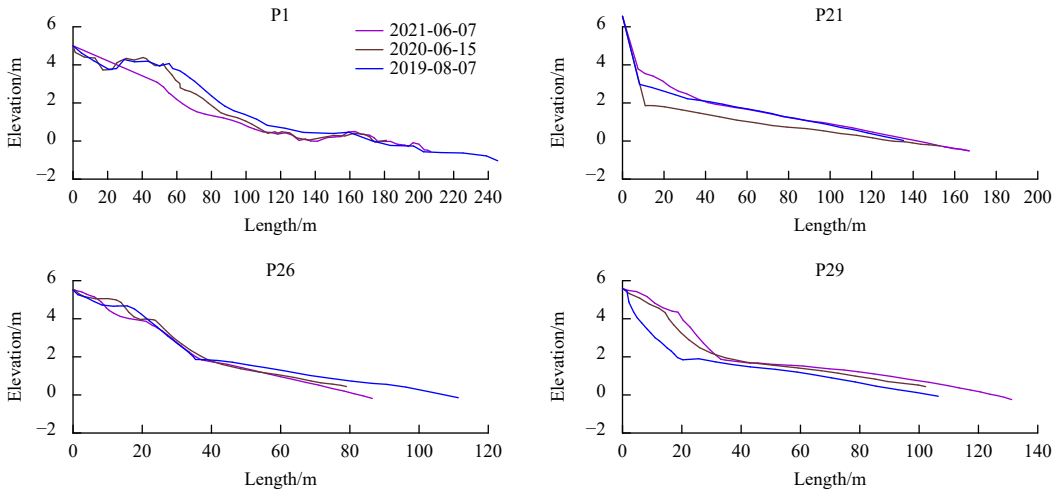

Fig. 5. Part of the summer profile during 2019 to 2021, see Supplementary information for a full profile of the study area.

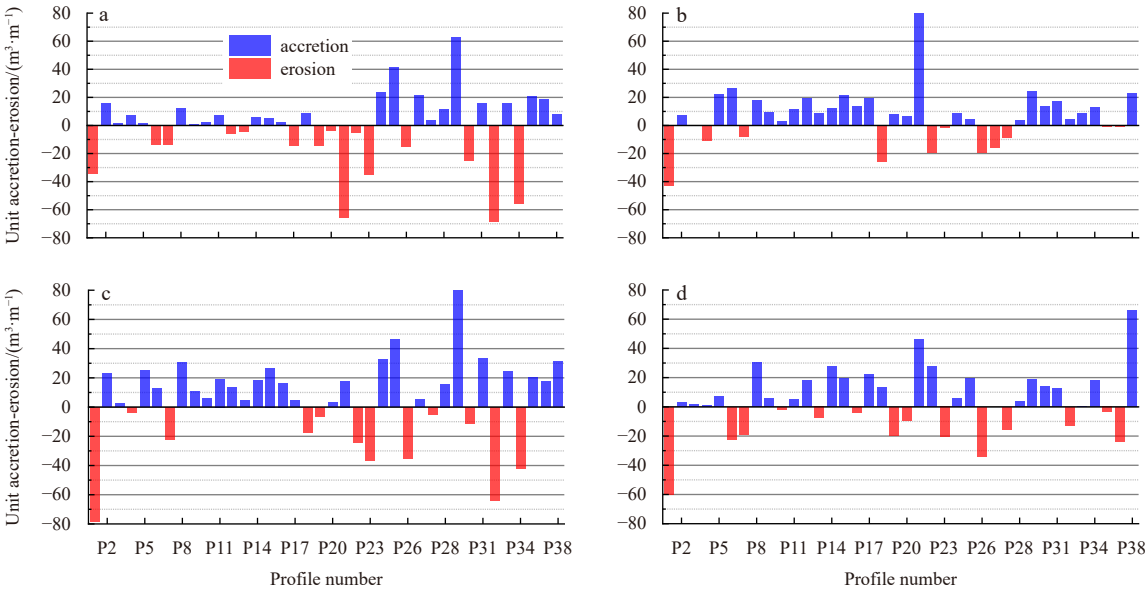

Fig. 6. Interannual erosion and accretion change under multiple scenarios during 2019 to 2021. Change in erosion and accretion from summer 2019 to summer 2020 (a), change in erosion and accretion from summer 2020 to summer 2021 (b), change in erosion and accretion from summer 2019 to summer 2021 (c), change in erosion and accretion from winter 2019 to winter 2020 (d).

3.4 *Seasonal variation in beach characteristics*

During the summer to winter transition (Fig. 7), W1 is intertidal erosion, supratidal and subtidal accretion, with a tendency for the slope of the beach to slow and a gradual change from accretion to erosion from north to south (e.g., P7, P15 in Fig. 7), but there are large differences in beach changes between the two seasonal transitions in Profile P21 (P21 in Fig. 5). In the southern four promontory beachs, erosion is intense, with a shift from erosion to accretion from north to south in W2 and W3, but with less accretion and greater accretion near Profile P29 (P26, P29 in Fig. 7). In contrast, the supratidal and intertidal zones of W4 and W5 are mostly erosional, with accretion occurring in the subtidal zone (P33, P36 in Fig. 7).

During the winter to summer transition (Fig. 8), the central part of W1 is clearly silted and eroded on both sides, but erosion differs in P21 and P22 (P21 and P22 in Fig. 4). The profile mainly shows a more stable hindshore, weak accretion in the intertidal zone, erosion in the subtidal zone, loss of subtidal sand bars and a small overall average amount of beach change (P7, P18 in Fig. 8). The four southern bays mostly show accretion, and the trend of change between the two seasonal shifts is the same, with the amount of accretion gradually increasing from north to south. The beaches mostly show accretion in the supratidal and intertidal zones and erosion in the subtidal zone, a few beaches are silted up overall, the profile slope becomes larger, some beaches form double beach shoulders, and the profile morphology is more variable (P28 in Fig. 8).

The two summer-winter and winter-summer single-width erosion and accretion volumes show significant differences (Fig. 9), with the summer-winter variation being mainly erosional, with mean single-width erosion volumes of 9.70 m^3/m and 3.92 m^3/m, respectively, and the winter-summer variation is mainly accretion, with mean single-width accretion volumes of 7.55 m^3/m and 10.81 m^3/m, respectively. W1 is less responsive to seasonal shifts than the four southern bays, with mean beach variation (MPC) ranging from 0.05 m to 0.31 m and 0.21 m to 1.15 m, respectively.

3.5 *Response of beaches to different typhoon landfall paths*

Under the action of Bailu, the Gulei Peninsula is generally eroded, with a few profiles showing accretion (Fig. 10a). In Bay W1, the single width erosion-accretion of each profile ranges from –9.92 m^3/m to 4.61 m^3/m (negative for erosion), and the average variation in beach profiles is 0.02–0.12 m. In the southern four bays, the overall change from accretion to erosion from north to south, with a large variation, the largest erosion is in Profile P31, southwards erosion increases, the profile forms double beach shoulders and intertidal erosion, and subtidal accretion is obvious. With sediment overtopping occurring in Profile P32, and the shoulder of the beach is eroded back towards the shore by approximately 35 m in Profile P34, with a maximum downwards erosion of 2 m.

Under the action of Mekkhala, W1 is relatively stable overall, with large variations in alluvial accretion in the southern four bays (Fig. 10b). The southern side of W1 shows significant accretion, with the amount of accretion gradually increasing from Profile P19 to the south, with the largest amount of accretion in Profile P21; the accretion height is nearly 1 m, and the single width is 99.09 m^3/m. The northern part of the four southern bays experiences accretion, and the southern part experiences erosion, W2 and W3 change from accretion to erosion from north to south, the profile morphology changes considerably, the profile beach shoulders are eroded, and the double beach shoulders recede (P26, P27). The Profile P29 is the most eroded, the lower erosion reaches 1.3 m, and the single width erosion is 60.24 m^3/m. The Profile W4 changes in line with W2 and W3, and the Profile W5 changes less.

Under the action of Lupit, W1 beach gradually transitions from overall erosion (P2, P3) to less overall change (P9–P17) from north to south, eventually changing to a state of overall accretion (P20, P21), with very high accretion on the southern side (Fig. 10c, P20, P21). In the southern four bays, the northern headland is silted, and the southern headland is eroded. The W2, W3 and W4 beaches follow the same overall trend, with W5 responding more to Lupit, with slight accretion in the supratidal zone and erosion in the intertidal and subtidal zones in Profiles P36 and P37, with a single width erosion of 26.38–29.13 m^3/m.

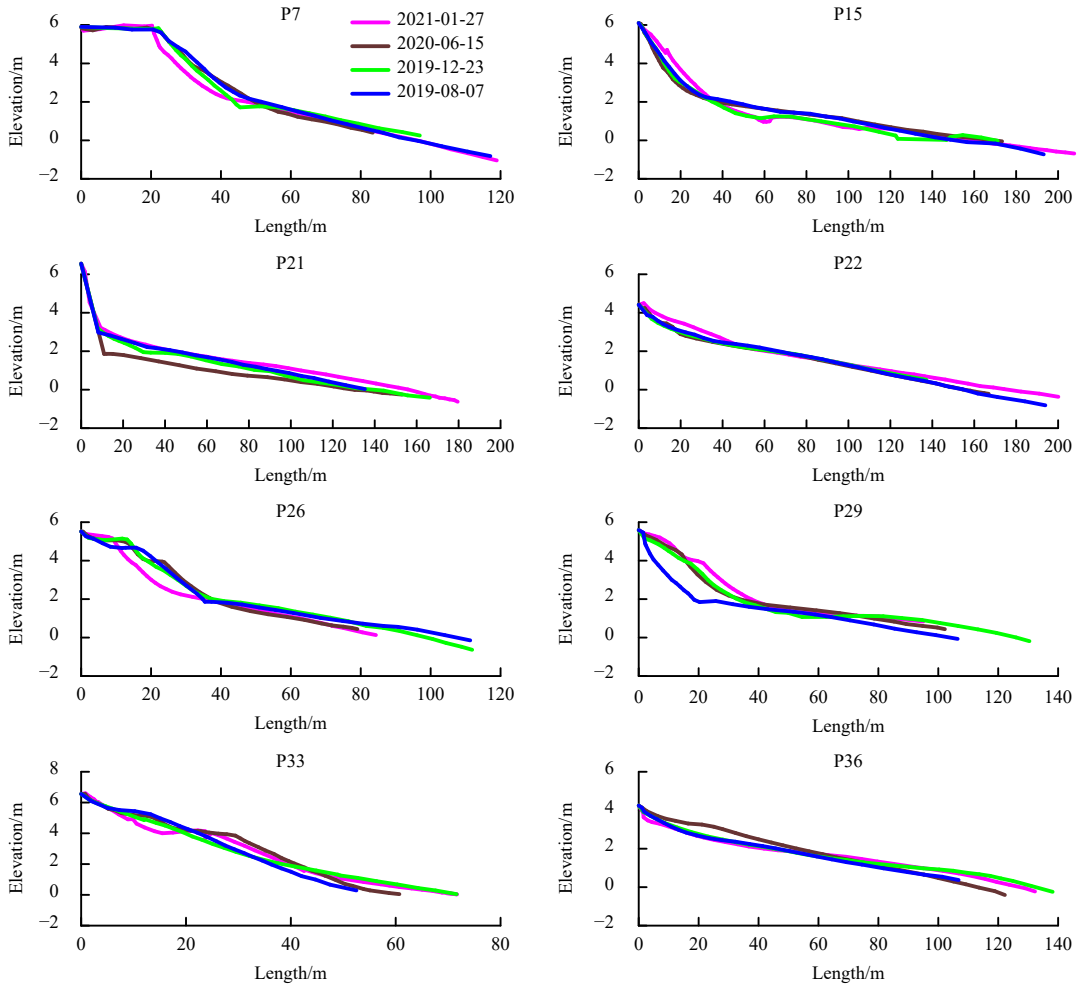

Fig. 7. Summer to winter profile during 2019 to 2021, see Supplementary information for a full profile of the study area.

4 Discussion

4.1 *Characteristics of beach geomorphology in response to the monsoon*

The distribution of beach sediment particles is commensurate with the intensity of wave action (Cai, 1989; Yang et al., 2018). When waves are pushed ashore into shallow water, the waves are deformed by bottom friction and wave breaks are formed. When wind and waves are high, the beach will be scoured in the intertidal zone under the action of the upwelling current, and the scoured sand particles will be carried to the subtidal zone by the return current, which is larger than normal. Some of the larger particles will be deposited directly near the high tide zone, making the profile show intertidal erosion, accretion of the upper and lower tidal zones, and even sand dams near the subtidal zone, developing a storm profile. When the wind and waves are small, the dynamic effect gradually decreases, and the sediment lifted by the breaking waves is carried to the shore beach by the onshore current. More sediment will be deposited gradually in the foreshore area of the shore beach so that the shore beach shoulder is restored, and the subtidal sand bar is eroded, developing a surge profile.

During the transition from summer to winter, the NE wind and waves gradually increase (Fig. 11a), the coastal dynamics are strong, the lower and middle parts of the Futou Bay are nearly vertically incised by the deviated E wind and waves, which is conducive to lateral sand transport, the intertidal zone is scoured by the upwelling current, and the particles are carried by the return current near the subtidal zone (Fig. 11c). The shore section is mostly eroded and shows a typical sand bar-type profile. The gradual increase in wave incidence angle towards the south causes the coastal current to be one of the main drivers of sand transport along the shore (Wang et al., 2001). The coastal current causes a north-south coastal transport of sand in the lower part of Futou Bay, which gradually accumulates at Profiles P21 and P22, where the drainage channel extends approximately 170 m out to sea, favouring the southwards transport of sand to accumulate near Profile P21, while the opposite trend occurs in the change from winter to summer. The sheltering of the northern part of Futou Bay by the Liu'ao Peninsula and the dissipative effect of the fish rafts, combined with the input of riverine material, has resulted in a small amount of accretion in the upper shore section of Futou Bay. In the south, the four bays are nearly parallel to the direction of wave incidence in winter, which facilitates the transport of sediment from north to south along the shore, and under the action of strong waves, the shoulder of the beach is directly eroded or even disappears, and some of the eroded sediment is carried to the subtidal zone, which forms a pattern of "upper erosion and lower accretion". Blocked by the headland or reef in the south, a large amount of sediment will gradually accumulate in the wave shadow area on the right side of the headland (Figs 11a, c). The large reefs in W4 and W5 block the incoming

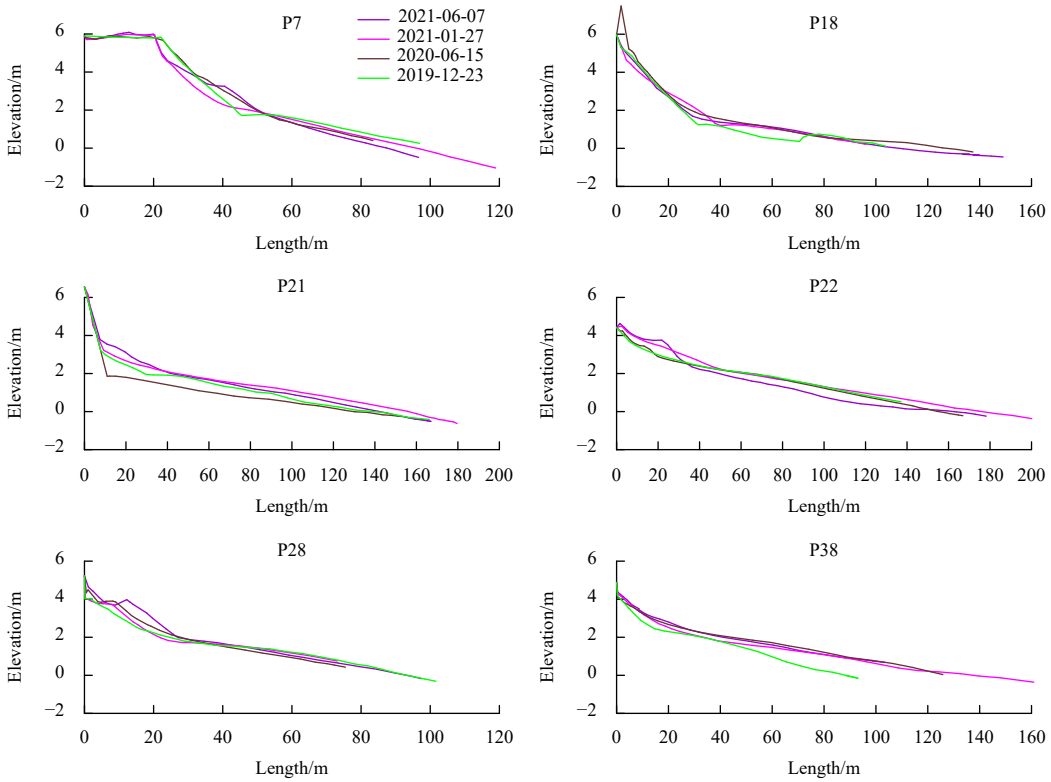

Fig. 8. Winter to summer profile during 2019 to 2021, see Supplementary information for a full profile of the study area.

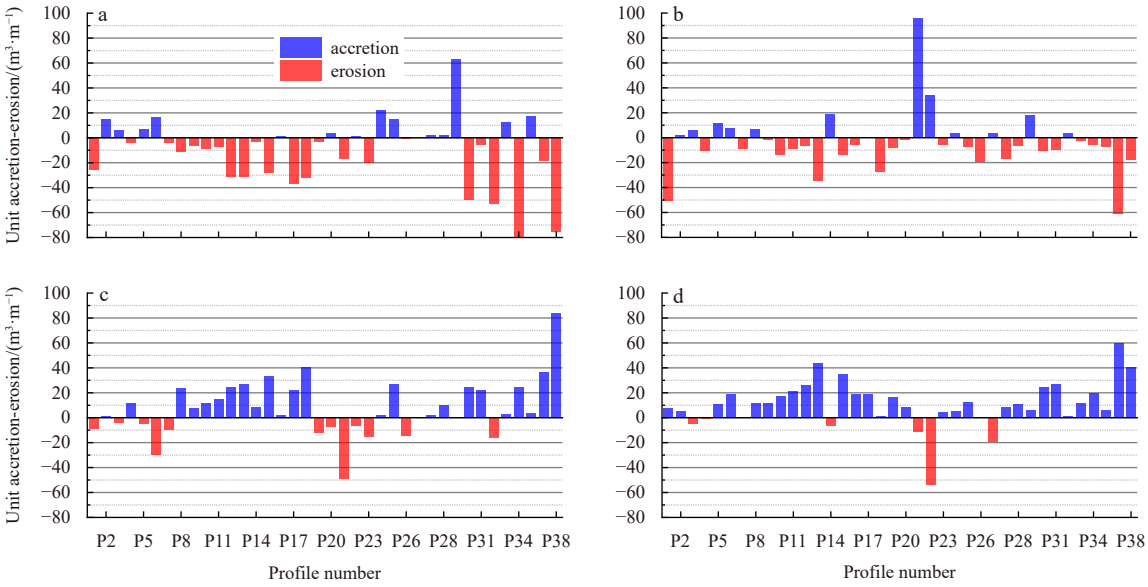

Fig. 9. Erosion and accretion variation under seasonal change during 2019 to 2021. Change in erosion and accretion from August 2019 to December 2019 (a), change in erosion and accretion from June 2020 to January 2021 (b), change in erosion and accretion from December 2019 to June 2020 (c), change in erosion and accretion from January 2021 to June 2021 (d).

sand on the north side, making the bay mainly erosional under strong wave action.

When changing from winter to summer, the wind and waves in the study area decrease, and the waves change to the S-direction (Fig. 11b), forming coastal sand transport from south to north, with the direction of wave incidence nearly parallel to the south side of Futou Bay, which is blocked by the Ao'tou Mountains and therefore shows weak erosion. In the middle of Futou Bay, the intertidal zone gradually silts up, and the beach becomes more dissipated by the combined effect of S-direction waves and estuarine runoff input, forming a surge profile. The beach becomes more dissipated, creating a swell profile. In the south, the four promontory beachs are nearly vertically influenced by the S-directional waves, which is conducive to the lateral sand transport of the beach. The beach profile changes greatly, and the sediment in the subtidal zone and outside the shoreline

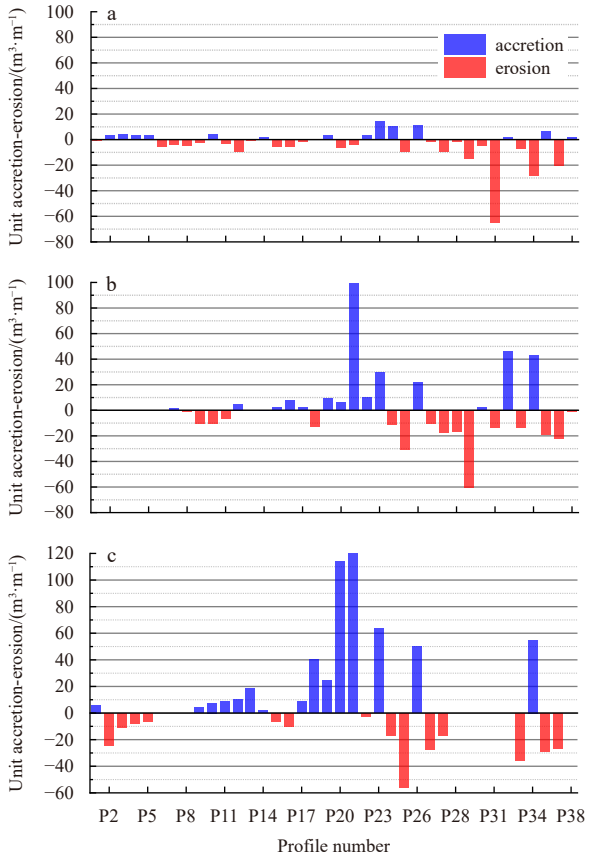

Fig. 10. Changes in erosion and accretion after the effects of Bailu (a), change in erosion and accretion after the effects of Mekkhala (b), change in erosion and accretion after the effects of Lupit (c).

is carried to the foreshore by the shoreward flow and is gradually deposited so that the beach develops into a beach shoulder, and some shore sections form a double beach shoulder (Figs 11b, d).

Interannually and even over long periods, the study area is influenced by the NE normal wave direction, which results in the north-to-south coastal transport of sand (Cai, 1989), and by the influence of the Liu'ao Peninsula and the Caiyu Islands, which weaken the wave energy in the NE direction (Cai, 1989), favouring sediment accumulation. The dissipation of wave energy from the large area of fishing rafts in the bay has resulted in the central part of Futou Bay showing continuous accretion over the years, with the shoreline continuously advancing seaward (Cai et al., 2006). The northern and southern parts of Futou Bay are in the open shore section, which is subject to the vertical incidence of NE waves and strong hydrodynamic forces acting directly on the beach, resulting in greater beach erosion. The serious destruction of vegetation along the backshore of this shore section, the large-scale modification of coastal dunes (Cai et al., 2006) and the alteration and expansion of human-made structures have caused major changes in the hydrodynamics of this shore section, further exacerbating coastal erosion.

4.2 *Characteristics of beach landforms in response to typhoons*

The response of beach morphology and type to tropical storms varies greatly (Basco, 1996; Cooper et al., 2004), with shoreline alignment, storm path, and landfall distance being important factors influencing the response of beach features to storms (Cai et al., 2002; Bauer et al., 2009; Guo et al., 2018, 2019; Hu et al., 2021), and beaches in different locations in the same region have different response characteristics to storms (Peng et al., 2008).

The wind direction was NNE, and the sheltering effect of the Liu'ao Peninsula made Futou Bay less responsive to Bailu, with an average change in beach profile of only 0.02–0.12 m. Under the effect of the NNE wind direction, the four southern bays formed strong shore waves, and the storm surge eroded the beach shoulder and scoured the supratidal zone, causing some sediments to accumulate in the subtidal zone and forming a storm profile. The strong offshore waves and storm surge erode the beach shoulders and scour the supratidal zone, causing some sediments to accumulate in the subtidal zone and forming a storm profile. The southern beaches show overall erosion due to their closer proximity to the typhoon.

Typhoon Mekkhala made landfall in Da'ao Bay to the northeast of the study area, and the study area was within a force 10 wind circle from one hour before to one hour after landfall, with large changes in wind direction before and after landfall. The upper and middle sections of Futou Bay were sheltered by the Liu'ao Peninsula, which blocked the N-directional winds and waves, making the upper and middle sections of Futou Bay more stable. The lower section of the bay was affected by N-driven waves, and a large amount of sediment was transported to the southern headland (P21) for accumulation. Before the typhoon made landfall, the four southern bays were mostly affected by offshore waves, and the beach shoulders were eroded and transported seaward, with some sediments accumulating in the subtidal zone. After the typhoon made landfall, the wind direction gradually changed to WNW, and the wind and waves caused the south side of the peninsula to form a south-to-north coastal sand transport, which was partially blocked by the southern headlands and reefs, thus causing the four southern bays to change from siltation to erosion.

Although the storm was less intense, it had a greater impact on the study area as it crossed the entire Gulei Peninsula. As Lupit ran from east to west across the Gulei Peninsula, the wind and waves induced by Lupit had a direct effect on the entire study area, and the sheltering effect of the Liu'ao Peninsula on Futou Bay was not effective. Before the landfall of Lupit, the beach of Futou Bay was sheltered by the Caiyu Islands, and the coastal sand transport from south to north was relatively small. After the landfall of Lupit, the NW wind and waves acted on Futou Bay and Jiuzhen Harbour, causing a large amount of sediment to be transported southwards, which was blocked by the southern headland, and a large amount of sediment accumulated in the southern part of Futou Bay. In the four southern bays, before the landfall of Lupit, the sediments in the middle and subtidal zones were transported to the upper tidal zone by the shoreward flow, while the action of the SE wave in the southern headlands also produced a northwards coastal transport of sand, which facilitated the accretion of sediments on the eastern side of the headlands. As Lupit moved northwards, it had little impact on the four southern bays due to sheltering of the land area.

4.3 *Characteristics of the differential response of beach material to hydrodynamic forces*

4.3.1 *Differential response of wave energy under different hydrodynamic conditions*

Wave breaking causes strong water turbulence with high energy and has a significant impact on beaches (Qi et al., 2009; Liu

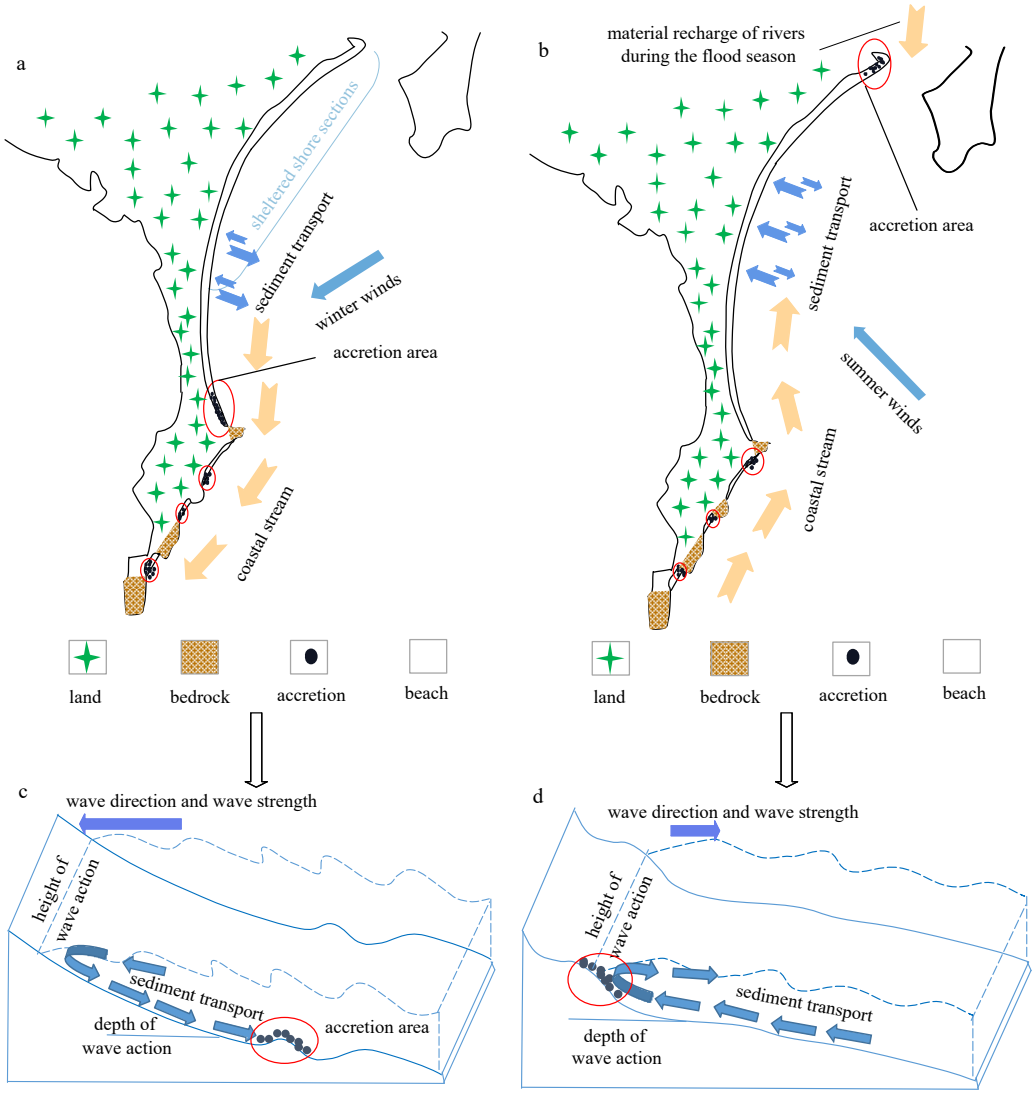

Fig. 11. Changes in beach geomorphology on the Gulei Peninsula under winter and summer wave action.

et al., 2021, 2022b). Calculating the amount of single width siltation for 11 conditions in the study area under seasonal, interannual and extreme conditions reflects the variability in wave energy under different hydrodynamic conditions (Fig. 12). The net change caused by Severe Tropical Storm Bailu, which was the stronger storm and farther away from the study area, was the smallest (A1). The net change caused by Typhoon Mekkhala, which was the strongest storm and closer to the study area, was similar to the seasonal change. Tropical Storm Lupit, which was the weakest storm and closest to the study area, had the largest impact (A3), with a net change greater than two years, more than three times that of Bailu. The net change in the seasonal shift is approximately 650 m^3/m, a nonsignificant difference, while the net change in the interannual variability is much greater, with an interannual much smaller than the interannual variability. When storms are extremely close together, the storm intensity, although small, produces much greater flushing and accretion than conventional dynamic conditions and even greater than the effect of 1–2 years of conventional hydrodynamic production (Basco, 1996; Cai et al., 2004; Shu et al., 2019), and the effect of storm distance is greater than the effect of storm intensity on the beach.

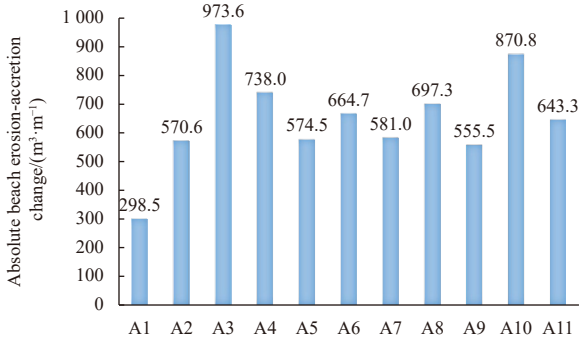

Fig. 12. The amount of absolute beach erosion-accretion change under different factors; A1–A11 represent the change in gross beach erosion accretion under Severe Tropical Storm Bailu, under Typhoon Mekkhala, under Tropical Storm Lupit, summer 2019 to winter 2019, summer 2020 to winter 2020, winter 2019 to summer 2020, winter 2020 to summer 2021, summer 2019 to summer 2019, summer 2020 to summer 2021, summer 2019 to summer 2021, winter 2019 to winter 2020, respectively.

4.3.2 *Differential response of beach geomorphology in different regions*

There are many dynamic factors that affect beach geomorphology, such as waves, tides and storm surges (Rosen, 1978; Chen, 1995; Ding et al., 2015). The variation in responses to different hydrodynamic conditions in different locations is reflected by calculating the amount of profile elevation change, which is an important characterization of the intensity of beach storm response (Qi et al., 2010). Headlands and the sheltering effect of islands reduce the wave energy transferred to the nearshore, resulting in less sloping and dissipated beaches, while beaches in open sections have higher nearshore wave energy and tend to develop steeper beaches (Chen and Chen, 2002).

The central part of Futou Bay is sheltered by the Liu'ao Peninsula, and the many fishing rafts and the wide and gentle beach surface effectively dissipate wave energy, resulting in less wave energy acting directly on the central part of Futou Bay and relatively small average changes in the beach profile. In the northern part of Futou Bay, runoff carries sediment that is easily deposited there, and the high variability in the beach profile at this location is closely related to the runoff volume of the river during the rich and dry periods (He, 2020). The southern part of Futou Bay is in the open section, where the wave energy acting on this area is higher and the beach variability is greater than in the central part of Futou Bay. The four southern bays differ greatly in development scale from Futou Bay, and the southern headland has less buffer space and greater variation in profile elevation, with the most dramatic variation seen in W4 (Fig. 13). In addition, as the alignment of the southern four bays is nearly parallel to the normal wave direction in the study area, the headland bays are more prone to steep slope shaping due to the frequent alternating sediment activity under the influence of the normal wave direction. The field survey found that the W4 beach is short, with an average width of approximately 80 m. At high water levels, the swell zone is narrow, and the increased water depth also results in less energy dissipation in wave propagation, with more energy concentrated in a small area (Fig. 14b), which has an unusually strong effect on the upper beach (Qi et al., 2010), making the W4 beach extremely unstable.

In summary, there is some variability in the response of different areas of beach to different hydrodynamics, with beaches with large headland developments and dissipated beaches tending to be more stable. Beaches in sheltered sections are less susceptible to erosion than those in open sections.

5 Conclusions

(1) Gulei Beach shows clear seasonal variation characteristics, mainly manifested as summer accretion and winter erosion. The promontory-straight beach (Futou Bay) is generally stable and responds weakly to seasonal changes. Obvious accretion changes occur near the estuary and the southern headland, while the southern headland shows winter erosion and summer accretion. The southern headland is more responsive to seasonal variation, with erosion dominating in winter, and a clear upwash and downwash period, which is the opposite in summer.

(2) There is variability in the impact of typhoons on beaches from different landfall paths. The response of Futou Bay to the three typhoons varied considerably, with the northern part of Futou Bay being more stable and the southern part being more silted up, and Futou Bay gradually changed from erosion to accretion from north to south. The amount of accretion was extremely large, with the response of Futou Bay being extremely large due to the direct landfall of the third typhoon. The response of the southern headland bays to the three different typhoons is similar, with each bay showing a shift from accretion to downward erosion from north to south, with the northern side of the barrier showing unusual accretion when blocked by islands or reefs.

(3) The responses of beaches in different regions of the study area to conventional and extreme hydrodynamic conditions vary considerably, with W1 being relatively stable and W2–W5 being more responsive. W4 was particularly responsive in relation to the width, scale and orientation of the headland bay and the length of the beach.

(4) At medium to long time scales, Futou Bay is relatively stable overall, showing more obvious cyclical changes, with obvious erosion hotspots due to human activities but then returning to normal. Obvious accretion occurs near the top of the bay, with the top of the bay being the boundary between obvious accretion and erosion on the north and south sides, respectively.

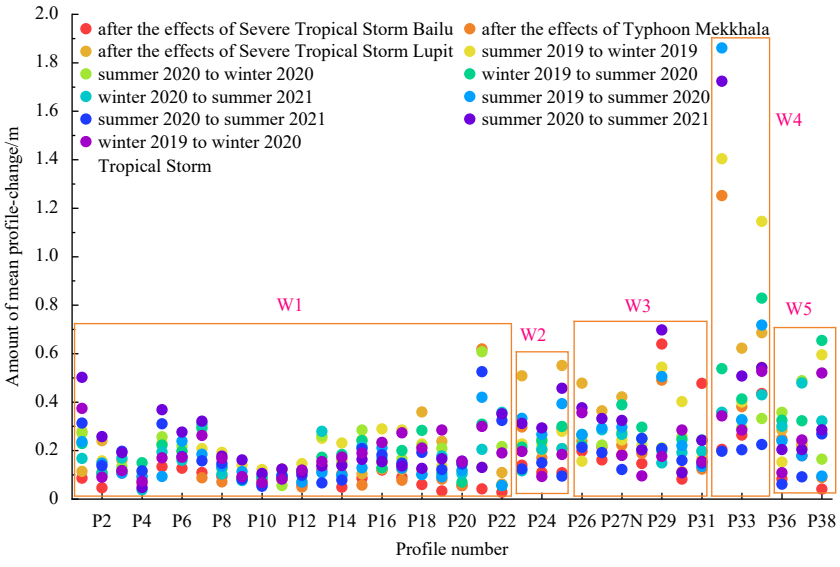

Fig. 13. Amount of elevation change in profiles at different locations.

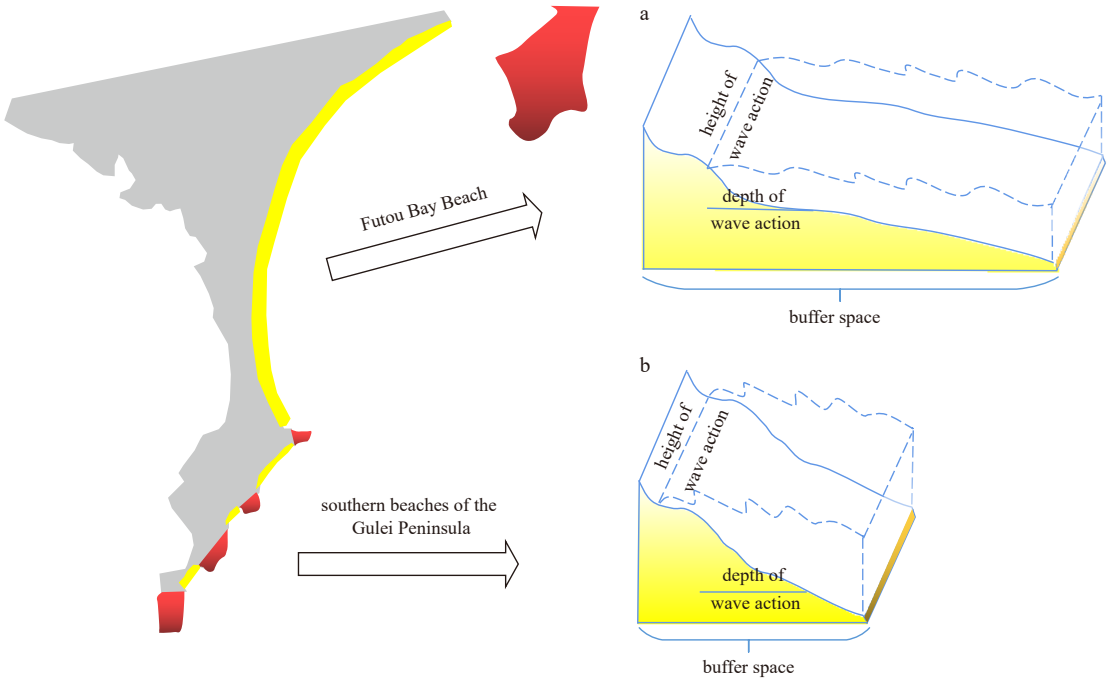

Fig. 14. Geomorphological changes in two different beach types, the beach is wide and gentle (a), and the beach is narrow and steep (b).

References

Allen J R L. 2000. Morphodynamics of Holocene salt marshes: a review sketch from the Atlantic and southern North Sea coasts of Europe. Quaternary Science Reviews, 19(12): 1155–1231, doi: 10.1016/S0277-3791(99)00034-7

Bagnold R A. 1940. Beach formation by waves: some model experiments in a wave tank. Journal of the Institution of Civil Engineers, 15(1): 27–52, doi: 10.1680/ijoti.1940.14279

Basco D R. 1996. Erosion of beaches on St. Martin Island during hurricanes Luis and Marilyn, September 1995 (Lessons for communities with beach-driven tourist economies). Shore & Beach, 64(4): 15–20

Bascom W N. 1951. The relationship between sand size and beach-face slope. Eos, Transactions American Geophysical Union, 32(6): 866–874, doi: 10.1029/TR032i006p00866

Bauer B O, Davidson-Arnott R G D, Hesp P A, et al. 2009. Aeolian sediment transport on a beach: surface moisture, wind fetch, and mean transport. Geomorphology, 105(1–2): 106–116, doi: 10.1016/j.geomorph.2008.02.016

Cai Aizhi. 1989. Beach cycle and coastal engineering. The Ocean Engineering (in Chinese), 7(3): 57–64, doi: 10.16483/j.issn.1005-9865.1989.03.006

Cai Feng, Cao Chao, Qi Hongshuai, et al. 2022. Rapid migration of mainland China's coastal erosion vulnerability due to anthropogenic changes. Journal of Environmental Management, 319: 115632, doi: 10.1016/j.jenvman.2022.115632

Cai Feng, Lei Gang, Su Xianze, et al. 2006. Study on process response of Fujian beach geomorphology to typhoon Aere. The Ocean Engineering (in Chinese), 24(1): 98–109, doi: 10.16483/j.issn.1005-9865.2006.01.016

Cai Feng, Su Xianze, Cao Huimei, et al. 2005. Analysis on morphodynamics of sandy beaches in South China. Haiyang Xuebao (in Chinese), 27(2): 106–114

Cai Feng, Su Xianze, Liu Jianhui, et al. 2009. Coastal erosion in China under the condition of global climate change and measures for its prevention. Progress in Natural Science, 19(4): 415–426, doi: 10.1016/j.pnsc.2008.05.034

Cai Feng, Su Xianze, Xia Dongxing. 2004. Study on the difference between storm effects of beaches on two sides of the Tropical Cyclone Track-taking the responses of beaches to No. 0307 Typhoon Imbudo as an example. Advances in Marine Science (in Chinese), 22(4): 436–445

Cai Feng, Su Xianze, Yang Shunliang, et al. 2002. A rapid response to 9914 typhoon-induced storm wave force made by the beach profiles of Xiamen Island. The Ocean Engineering, 20(2): 85–90, doi: 10.16483/j.issn.1005-9865.2002.02.016

Cao Chao, Cai Feng, Qi Hongshuai, et al. 2022a. Coastal erosion vulnerability in mainland china based on fuzzy evaluation of cloud models. Frontiers in Marine Science, 8: 790664, doi: 10.3389/fmars.2021.790664

Cao Chao, Zhu Kai, Cai Feng, et al. 2022b. Vulnerability evolution of coastal erosion in the Pearl River Estuary great bay area due to the influence of human activities in the past forty years. Frontiers in Marine Science, 9: 847655, doi: 10.3389/fmars.2022.847655

Chen Zisheng. 1995. Analysis of the dynamic characteristics and stochastic simulation on variations of beach volumes. Acta Oceanologica Sinica, (3): 393–403

Chen Jiyu, Chen Shenliang. 2002. Estuarine and coastal challenges in China. Marine Geology Frontiers (in Chinese), 18(1): 1–5

Cooper J A G, Jackson D W T, Navas F, et al. 2004. Identifying storm impacts on an embayed, high-energy coastline: examples from western Ireland. Marine Geology, 210(1–4): 261–280

Davies J L. 1958. Wave refraction and the evolution of shoreline curve. Geographical Studies, 5(2): 1–14

Diez J, Cohn N, Kaminsky G M, et al. 2018. Spatial and temporal variability of dissipative dry beach profiles in the Pacific Northwest, U.S.A. Journal of Coastal Research, 34(3): 510–523, doi: 10.2112/JCOASTRES-D-17-00149.1

Ding Dong, Yang Jichao, Li Guangxue, et al. 2015. A geomorphological response of beaches to Typhoon Meari in the eastern Shandong Peninsula in China. Acta Oceanologica Sinica, 34(9): 126–135, doi: 10.1007/s13131-015-0644-5

Folk R L, Ward W C, 1957. Brazos River bar [Texas]; A study in the significance of grain size parameters. Journal of Sedimentary Research, 27(1): 3–26

Guo Junli, Shi Lianqiang, Chen Shengliang, et al. 2019. Response of Dongsha beach in Zhoushan to continuous storms based on Argus images. Oceanologia et Limnologia Sinica (in Chinese), 50(4): 728–739

Guo Junli, Shi Lianqiang, Chen Shengliang, et al. 2022. Dynamic variations of different sedimentary geomorphology of sandy and

gravel embayed beaches on the Zhujiajian Island during typhoon season. Journal of Tropical Oceanography (in Chinese), 41(4): 82–96

Guo Junli, Shi Lianqiang, Tong Xiaoling, et al, 2018. The response to tropical storm Nakri and the restoration of Dongsha Beach in Zhujiajian Island, Zhejiang Province. Haiyang Xuebao (in Chinese), 40(9): 137–147

He Zhuolun, 2020. Analysis of river sediment variation and its impact in Qinghai Lake river basin. Yellow River (in Chinese), 42(10): 23–28

Hsu J R C, Evans C. 1989. Parabolic bay shapes and applications. Proceedings of the Institution of Civil Engineers, 87(4): 557–570, doi: 10.1680/iicep.1989.3778

Hu Taihuan, Li Zhiqiang, Zhu Shibing, et al. 2021. Dynamic variation characteristics of beach profile along southern coast of Qiongzhou Strait. Journal of Applied Oceanography (in Chinese), 40(4): 678–687

Karunarathna H, Horrillo-Caraballo J M, Ranasinghe R, et al. 2012. An analysis of the cross-shore beach morphodynamics of a sandy and a composite gravel beach. Marine Geology, 299–302: 33–42, doi: 10.1016/j.margeo.2011.12.011

Komar P D. 1998. Beach Processes and Sedimentation. 2nd ed. Englewood Cliffs: Prentice-Hall

Kuriyama Y, Yanagishima S. 2016. Investigation of medium-term barred beach behavior using 28-year beach profile data and Rotated Empirical Orthogonal Function analysis. Geomorphology, 261: 236–243, doi: 10.1016/j.geomorph.2016.03.002

Li Guangtian, Fu Wenxia. 1992. Coastal erosion and its hazards in China. Marine Environmental Science (in Chinese), 11(1): 53–58

Li Guqi, Peng Jun, Cai Feng, et al. 2007. Responses of sandy beaches on sand bar-lagoon shores to typhoon. Marine Geology Frontiers, 23(8): 14–18, doi: 10.3969/j.issn.1009-2722.2007.08.004

Liu Jianhui, Cai Feng, Qi Hongshuai, et al. 2014. Geomorphologic features of the beach-dune system along Fujian coast. Marine Geology & Quaternary Geology (in Chinese), 34(1): 45–56

Liu Yong, Chen Benqing, Liu Lejun, et al. 2016. Coastal erosion and its cause analysis in different spatial temporal scales based on multi sources data in Dongshan Island of Fujian Province. Haiyang Xuebao (in Chinese), 38(3): 98–110

Liu Tiewei, Qu Ke, Huang Jingxuan, et al. 2021. Numerical investigation of hydrodynamic characteristics of solitary wave over permeable fringing reef. Chinese Journal of Hydrodynamics (in Chinese), 36(2): 180–191, doi: 10.16076/j.cnki.cjhd.2021.02.004

Liu Xinglu, Xu Sheng, Luo Xiaofeng, et al. 2022a. Seasonal variation characteristics and causes of headland-bay beaches: a case study of Guanhu beach. The Ocean Engineering (in Chinese), 40(4): 44–52, doi: 10.16483/j.issn.1005-9865.2022.04.006

Liu Wenshuai, Zheng Jianguo, Zhang Chongyue, et al. 2022b. Analysis of turbulent energy and energy loss caused by wave breaking on different beach shapes. Transactions of Oceanology and Limnology (in Chinese), 44(1): 1–8, doi: 10.13984/j.cnki.cn37-1141.2022.01.001

Luo Shilong, Cai Feng, Wang Houjie. 2013. Development of coastal erosion and management. Advances in Earth Science (in Chinese), 28(11): 1239–1247

Luo Xianlin, Li Chunchu, Luo Zhangren. 2000. Erosion and abandonment of the Nandu River Delta, Hainan Island. Haiyang Xuebao (in Chinese), 22(3): 55–60

McCormick M E. 1993. Equilibrium shoreline response to breakwaters. Journal of Waterway, Port, Coastal, and Ocean Engineering, 119(6): 657–670

Medina R, Losada M A, Losada I J, et al. 1994. Temporal and spatial relationship between sediment grain size and beach profile. Marine Geology, 118(3–4): 195–206, doi: 10.1016/0025-3227(94)90083-3

Miller J K, Dean R G. 2007a. Shoreline variability via empirical orthogonal function analysis: Part I temporal and spatial characteristics. Coastal Engineering, 54(2): 111–131, doi: 10.1016/j.coastaleng.2006.08.013

Miller J K, Dean R G. 2007b. Shoreline variability via empirical orthogonal function analysis: Part II relationship to nearshore conditions. Coastal Engineering, 54(2): 133–150, doi: 10.1016/j.coastaleng.2006.08.014

Mimura N, Shimizu T, Horikawa K. 2010. Laboratory study on the influence of detached breakwater on coastal change. In: Coastal Structures'83. Arlington, TX: American Society of Civil Engineers

Peng Jun, Cai Feng, Li Guqi, et al. 2008. Response characteristic to the typhoon of sandy beach on the inshore between capes in Fujian. Journal of Oceanography in Taiwan Strait (in Chinese), 27(1): 87–91

Qi Hongshuai, Cai Feng, Lei Gang, et al. 2010. The response of three main beach types to tropical storms in South China. Marine Geology, 275(1–4): 244–254, doi: 10.1016/j.margeo.2010.06.005

Qi Hongshuai, Cai Feng, Su Xianze, et al. 2009. Study on geomorphologic process of beaches under tropical storm action Taking the effect of No. 0604 tropical storm Bylis on Banyue Bay beach in Fujian Province, China as an example. Haiyang Xuebao (in Chinese), 31(1): 168–176

Ravens T M, Thomas R C, Roberts K A, et al. 2009. Causes of salt marsh erosion in Galveston Bay, Texas. Journal of Coastal Research, 25(2): 265–272, doi: 10.2112/07-0942.1

Rosen P S. 1978. Beach processes and sedimentation. Paul D. Komar. The Journal of Geology, 86(1): 155

Shepard F P, Inman D L. 1950. Nearshore water circulation related to Bottom topography and wave refraction. Eos, Transactions American Geophysical Union, 31(2): 196–212, doi: 10.1029/TR031i002p00196

Shu Fangfang, Cai Feng, Qi Hongshuai, et al. 2019. Study on various response to typhoon of nourished beaches with different sediments. Haiyang Xuebao (in Chinese), 41(7): 103–115

Tian Huibo, Yin Ping, Yang Fanlin. 2018. An analysis of erosional characteristics of the sandy coast in the eastern part of Wanning, Hainan. Marine Geology & Quaternary Geology (in Chinese), 38(4): 44–55, doi: 10.16562/j.cnki.0256-1492.2018.04.004

Vos K, Splinter K D, Harley M D, et al. 2019. CoastSat: A Google Earth Engine-enabled Python toolkit to extract shorelines from publicly available satellite imagery. Environmental Modelling & Software, 122, 104528: 1–7

Wang Guanglu. 2008. The study of bay beach restoration and nourishment [dissertation]. Xiamen: Third Institute of Oceanography of State Oceanic Administration

Wang Houjie, Yang Zuosheng, Li Ruijie, et al. 2001. Numerical modeling of the seabed morphology of the subaqueous Yellow River Delta. International Journal of Sediment Research, 4: 486–498

Wang Aijun, Ye Xiang, Shu Fangfanag, et al. 2011. Analysis of sediment grain size characteristics and siltation dynamics on the eastern shoreline of Gulei Peninsula, Fujian. In: Proceedings of the 15th China Marine (Offshore) Engineering Symposium (in Chinese). Taiyuan: Ocean Engineering Branch of the Chinese Ocean Society, 332–337

Wentworth C K, 1922. A scale of grade and class terms for clastic sediments. The Journal of Geology, 30(5): 377–392, doi: 10.1086/622910

Wright L D, Thom B G. 1977. Coastal depositional landforms: a morphodynamic approach. Progress in Physical Geography: Earth and Environment, 1(3): 412–459, doi: 10.1177/030913337700100302

Xia Jing. 2015. Study of the sedimentary structure, grain size characteristics and sedimentary environment of coastal dunes in Zhangpu County, Fujian Province (in Chinese)[dissertation]. Fuzhou: Fujian Normal University

Xia Dongxing, Wang Wenhai, Wu Guiqiu, et al. 1993. Coastal erosion in China. Acta Geographica Sinica (in Chinese), 48(5): 468–476

Xia Lihua, Wu Huiming, Liu Ming, et al. 2014. Characteristic analysis of storm surges along Fujian coast associated with tropical cyclones. Journal of Tropical Oceanography (in Chinese), 33(3): 40–45

Yang Yadi, Zheng Jianguo, Yue Shuai, et al. 2018. Experimental study on vertical differentiation of beach sand under wave action.

Periodical of Ocean University of China (in Chinese), 48(S1): 123–130, doi: 10.16441/j.cnki.hdxb.20180136

Young A P, Flick R E, Gutierrez R, et al. 2009. Comparison of short-term seacliff retreat measurement methods in Del Mar, California. Geomorphology, 112(3–4): 318–323, doi: 10.1016/j.geomorph.2009.06.018

Young I R, Sobey R J. 1980. A predictive model of tropical cyclone wind-waves. In: 7th Australasian Conference on Hydraulics and Fluid Mechanics. Brisbane: The University of Melbourne, 480–483

Yu Jitao, Chen Zisheng. 2009. Study progress of sandy coastal erosion. Tropical Geography (in Chinese), 29(2): 112–118, doi: 10.3969/j.issn.1001-5221.2009.02.002

Supplementary information:

Fig. S1. Profile morphological characteristics of P1 to P10 in the study area.

Fig. S2. Profile morphological characteristics of P11 to P20 in the study area.

Fig. S3. Profile morphological characteristics of P21 to P29 in the study area.

Fig. S4. Profile morphological characteristics of P30 to P38 in the study area.

The supplementary information is available online at https://10.1007/s13131-023-2225-3 and www.aosocean.com. The supplementary information is published as submitted, without typesetting or editing. The responsibility for scientific accuracy and content remains entirely with the authors.